

Rare-earth impurities in Co_2MnSi :

an opportunity to improve Half-Metallicity at finite temperatures

E. Burzo and I. Balazs

Babeş-Bolyai University Cluj-Napoca, RO-800084 Cluj-Napoca, Romania

L. Chioncel and E. Arrigoni

*Institute of Theoretical and Computational Physics,
Graz University of Technology, A-8010 Graz, Austria*

F. Beiuşeanu

Faculty of Science, University of Oradea, RO-410087 Oradea, Romania

Abstract

We analyse the effects of doping Holmium impurities into the full-Heusler ferromagnetic alloy Co_2MnSi . Experimental results, as well as theoretical calculations within Density Functional Theory in the Local Density Approximation generalized to include Coulomb correlation at the mean field level show that the holmium moment is aligned antiparallely to that of the transition metal atoms. According to the electronic structure calculations, substituting Ho on Co sites introduces a finite density of states in the minority spin gap, while substitution on the Mn sites preserves the half-metallic character.

I. INTRODUCTION

An important class of materials which are intensively studied in the field of spintronics are the so-called half-metallic ferromagnets. These materials are characterized by a metallic electronic structure for one spin channel, whereas, for the opposite spin direction, the Fermi level is situated within an energy gap [1, 2]. From a magnetic point of view, these compounds can be either ferro- or ferrimagnets. Quite generally, theoretical calculations based on the Local-Density Approximation (LDA) predict a perfect spin polarization at the Fermi level. Antiferromagnetic half-metals also exist, although this case is special since no symmetry relation connects spin-up and spin-down directions. The existence of half-metallicity in all three classes of magnetic orderings was predicted by *R. A. de Groot* and coworkers some years ago [1, 3, 4]. Since then, several possible half-metallic ferromagnetic (HMF) materials have been theoretically investigated by ab initio calculations, and some of them have been synthesized and experimentally studied.

Devices that exploit spin and charge of the electrons should operate at not too low temperatures. Unfortunately many half-metallic systems exhibit a dramatic suppression of spin-polarization well below room temperature [2, 5]. It is therefore important to study and to optimize temperature effects in half-metallic materials. There are several effects potentially responsible for the suppression of spin polarisation at finite temperature that can be taken into account in a theoretical calculation. The competition between hopping and local electron-electron interactions may produce spin disorder, which can be approximated as random intraatomic exchange interactions [6, 7]. These interactions modify the local magnetic moments and influence the spin polarization [8, 9]. The exchange interactions described by a Heisenberg-type Hamiltonian are also frequently used to discuss finite temperature magnetic effects. The sign and magnitude of exchange constants give information whether the spin structure is collinear or not [7, 10, 11]. Note that non-collinearity may be produced also by spin-orbit coupling. All the above mentioned mechanisms may be called spin-mixing effects [5, 12] and they may significantly influence the half-metallic character.

It is important to point out that in all metallic ferromagnets, the interaction between conduction electrons and spin fluctuations determines their physical properties. In half-metallic ferromagnets the presence of the gap in one of the spin channel determines the absence of spin-flip, or one-magnon scattering processes which modifies considerably the

electrons energy spectrum [2, 13, 14]. These electron-magnon interactions occur both in usual ferromagnets and in half-metals, with the difference that for the usual ferromagnets the states around the Fermi level are quasiparticles for both spin directions, while in half-metals an important role is played by incoherent - non-quasiparticle (NQP) - states [13, 14]. The origin of these NQP states is connected with spin-polaron processes: the spin-down low-energy electron excitations, which are forbidden for HMF in the one-particle picture, turn out to be possible as result of superpositions of spin-up electron excitations and virtual magnons [2, 14–16]. It was demonstrated that these states are important for spin-polarized electron spectroscopy [17], nuclear magnetic resonance [18], and subgap transport in ferromagnet-superconductor junctions (Andreev reflection) [19]. Recently, the density of NQP states has been calculated using an LDA+dynamical mean field theory (DMFT) approach [2, 20], for several materials such as the semi-Heuslers NiMnSb [21] and (NiFe)MnSb [22], the full Heuslers Mn₂VAI [23] and Co₂MnSi [24], the zinc-blende CrAs [25] and VAs [26] and the transition metal oxide CrO₂ [27], demonstrating their importance as the essential mechanism of depolarization in half-metals.

Among the Heusler half-metals, the full-Heusler Co₂MnSi [28–30] has been intensively studied experimentally as well as theoretically. This material is interesting as it shows a high Curie temperature and very little crystallographic disorder [31]. We showed that Co₂MnSi experiences a drastic spin depolarization [24] with increasing temperature. According to our calculations, depolarization is caused by the occurrence of non-quasiparticle states situated just above the Fermi level in the minority spin channel [2, 24]. In order to significantly reduce depolarization a strategy to eliminate the NQP states from the Fermi level is required. In other words, one should try to suppress finite-temperature magnonic excitations while at the same time preserving the minority spin gap. It was suggested that the substitution of a rare-earth (R) element within the Mn sublattice of NiMnSb would introduce gaps in the magnonic spectrum due to the impurity R(4*f*) - Mn(3*d*) coupling, possibly preserving the half-metallic gap [2, 32, 33]. In pure NiMnSb the ferromagnetic Curie temperature $T_C = 740\text{K}$ is determined by the strength of the Mn-Mn (3*d* – 3*d*) coupling [2, 10]. The strength of (3*d* – 4*f*) couplings in NiMn_{1-*x*}R_{*x*}Sb compounds, with R=Nd, Pm, Ho, U was discussed previously [2, 33]. A large 3*d* – 4*f* coupling was obtained for the case of Nd substitution, and the weakest coupling was realized in the case of Ho. For all rare-earth substitutions the electronic-structure calculations showed that the half-metallic gap is not

affected, and for temperatures smaller than the values of the $3d - 4f$ couplings, interaction will lock the Mn($3d$) magnetic moment fluctuation. As a consequence, it was concluded that Nd substitution is of practical importance for high-temperature applications [2], while half-metallicity with Ho substitutions would persist up to temperatures of around 4K as predicted by the calculation [32, 33].

For the case of Co_2MnSi , preliminary results showed that Ho can enter in the Co_2MnSi lattice [34]. Recently, *Rajanikanth et. al.* [35] showed that substituting Co with 1.25at% Nd results in a single L_{21} phase alloy with a thin layer of Nd-enriched phase boundaries. A suppression of electron-magnon scattering was experimentally observed [35].

As an ongoing investigation of impurity effects on the depolarization of conduction electrons in Co_2MnSi based alloy we analyze in this paper the possibility of substituting holmium in both Co or Mn lattice sites, as well as changes introduced in band structure of the parent compound. The first task is to analyze whether holmium can really replace Mn or Co in a $Fm\bar{3}m$ type structure. Consequently, we prepared samples in which the substitution at both transition metal sites was considered. X-rays and electron microscopy studies were carried out. Finally, the magnetic properties and band structures of the doped compounds were analyzed.

II. PHYSICAL PROPERTIES OF HO-DOPED Co_2MnSi SAMPLES

The $\text{Co}_2\text{Mn}_{1-x}\text{Ho}_x\text{Si}$ and $\text{Co}_{2-x}\text{Ho}_x\text{MnSi}$ alloys with nominal compositions $x = 0.05$ and $x = 0.1$ were prepared by arc melting the constituent elements under purified argon atmosphere. These were remelted several times in order to ensure a good homogeneity. The alloys were annealed at 900°C for 12 days. The X-ray analyses were performed by using a Brucker V8 diffractometer. Rietveld refinements were made by using the Topas code. Electron microscope studies were performed by using a JEOL type equipment. The compositions of the samples and distributions of the constituent elements were analysed. Magnetic measurements were made with an Oxford Instruments type equipment in fields up to 5 T and in the temperature range 4.2-1000 K.

A. Experimental results

The refined X-ray diffraction (XRD) spectra of $\text{Co}_2\text{Mn}_{1-x}\text{Ho}_x\text{Si}$ samples with $x = 0.05$ and $x = 0.1$ are plotted in Fig.1. The same type of spectra were obtained when Ho substitutes Co. The alloys crystallize in a cubic structure having $Fm\bar{3}m$ space group. As seen from Table I, the lattice parameters increase little when increasing holmium content. The linewidths of XRD spectra are a little larger in samples having a composition $x = 0.1$ as compared to those having $x = 0.05$. This can be correlated with a small deformation of the lattices as the holmium content increases.

The better agreement between the computed spectra and those experimentally determined, in $\text{Co}_2\text{Mn}_{1-x}\text{Ho}_x\text{Si}$ alloys is obtained when holmium substitutes manganese located in 4c sites, according to the starting composition. The goodness of fit (GOF) values are indeed worse (larger) if one assumes that Ho occupies cobalt 4a or 4b sites. On the other hand, the refinements of the crystal structures of $\text{Co}_{2-x}\text{Ho}_x\text{MnSi}$ samples showed GOF values rather close when Ho was considered either to replace cobalt or manganese. In addition, a further analysis of our data strongly suggests that holmium occupies lattice sites in Co_2MnSi sample, and does not sit in interstitial positions.

The compositions of the samples were determined by Scanning Electron Microscopy (SEM), for a surface area of $\approx 1\text{mm}^2$ and a depth from surface up to about 200\AA . The determined holmium content in samples having initial compositions $x = 0.05$ and 0.1 were $1.30 \pm 0.15\text{at}\%$ and $(2.7 - 2.8) \pm 0.30\text{at}\%$ respectively in both $\text{Co}_2\text{Mn}_{1-x}\text{Ho}_x\text{Si}$ and $\text{Co}_{2-x}\text{Ho}_x\text{MnSi}$ systems Figs.2a,b. These values are in agreement with the expected content of $1.25\text{at}\%$ and $2.5\text{at}\%$, respectively. The manganese contents in $\text{Co}_2\text{Mn}_{1-x}\text{Ho}_x\text{Si}$ were $22.8 \pm 0.7\text{at}\%$ ($x = 0.05$) and $22.0 \pm 0.6\text{at}\%$ ($x = 0.1$), while the cobalt content was close to $50\text{at}\%$ - Figs.2a,b. The above data suggest that holmium is distributed mainly in manganese sites in this compound.

On the other hand, in the case of $\text{Co}_{2-x}\text{Ho}_x\text{MnSi}$ samples there is a decrease of both cobalt and manganese content as compared to expected compositions, suggesting that holmium can occupy both these sites. The distribution of holmium atoms in the samples was also analysed. As example, we show in Figs.2c,d the SEM patterns of two manganese substituted samples. A random distribution can be seen, with no clustering effects.

The magnetizations isotherms, at 4.2K , are shown in Fig. 3. The determined saturation

magnetizations, M , per formula unit are given in Table II. The M values are smaller than the ones measured in Co_2MnSi , namely $5\mu_B$ [36], and decrease when increasing holmium content. This suggests that the holmium moments are antiparallely oriented to the cobalt and manganese ones. Therefore, the magnetization measurements are in agreement with the result of structural and compositional analysis and confirm that holmium atoms occupy lattice sites, and that their moment is antiparallely oriented to cobalt and manganese ones. A better agreement is obtained for a composition $x = 0.05$. For samples having higher holmium content a little deviation from the expected stoichiometry or a possible location of Ho in both Co and Mn lattice sites cannot be excluded. The analysis of thermal variations of magnetizations in low field, shows the presence of only one magnetic phase. The Curie temperatures of the Ho-doped samples are only minimally reduced with respect to that of Co_2MnSi ($T_c = 985$ K) as seen in Table I.

B. Electronic Structure of Ho doped Co_2MnSi

To compute the electronic structure we used the standard representation of the L2_1 structure with four inter-penetrating fcc sub-lattices. The atomic positions are $(0, 0, 0)$ for Co1, $(1/2, 1/2, 1/2)$ for Co2, and $(1/4, 1/4, 1/4)$ and $(3/4, 3/4, 3/4)$ for Mn and Si, respectively. We note that the Co1 and Co2 sites are equivalent. We used the experimental lattice constant $a = 5.65\text{\AA}$ and the linear muffin-tin orbital method (LMTO)[37] extended to include the mean-field Hubbard +U approximation (LDA+U) [38]. It is generally known that the LDA+U method applied to metallic compounds containing rare-earth elements, gives a qualitative improvement compared with the LDA not only for excited-state properties such as energy gaps but also for ground-state properties such as magnetic moments and interatomic exchange parameters. Therefore it is expected that it will provide a correct description for the narrow $\text{Ho}(4f)$ states, the minority spin gap and the $3d - 4f$ coupling in the Ho doped Co_2MnSi .

The origin of the minority band gap in the full Heusler alloy was discussed by *Galanakis et al.* [39]. Based on the LDA band-structure calculations for the undoped Co_2MnSi , it was shown that Co1 and Co2 couple forming bonding/anti-bonding hybrids. The $\text{Co1}(t_{2g}/e_g)$ - $\text{Co2}(t_{2g}/e_g)$ hybrid bonding orbitals hybridize with the $\text{Mn}(t_{2g}/e_g)$ manifold, while the Co-Co hybrid anti-bonding orbitals remain uncoupled due to their symmetry. The Fermi

energy is situated within the minority spin gap formed by the triply degenerate anti-bonding Co-Co(t_{2g}) and the double degenerate anti-bonding Co-Co(e_g) (Fig. 4). Due to the orbitals occupation, the majority spin channel has a metallic character, with a small density of states at the Fermi level. In agreement with previous [10, 11, 39, 40] calculations, an integer total spin magnetic moment of $5.00\mu_B$, and a minority spin gap of magnitude $0.42eV$ is obtained.

The behavior of the magnetic moment as a function of temperature in undoped Co_2MnSi was discussed in the framework of the LDA+DMFT method [24]. Both magnetisation and spin polarisation decrease with increasing temperature, although the latter decreases much faster. Above the Fermi level, non-quasiparticle (NQP) states [2, 14–16] are present, which influence significantly the finite temperature properties [24].

We have performed LDA+U calculations for different values of the average Coulomb interaction parameter U and different sizes of the unit cell, in order to investigate the sensitivity of the results with respect to these parameters. The parameters study was performed for the energetically most favorable Ho substitution, namely the replacement of a Mn atom by Ho with an antiparallel coupling of the Ho spin moment with respect to the Mn itinerant electrons spin moment. For all our values of U a half-metallic solution is obtained with a minority gap having similar width as in the spin polarized LDA calculation, however depending on the strength of U the Fermi level moves towards the middle of the gap. In Fig. 5 we present the computed value of the Ho spin moments together with the difference between the bottom of the conduction band (E_B) and the Fermi level $E_B - E_F$ as a function of the average coulomb parameter U . As one can see there is no significant dependence in the studied range of the U parameter $8 - 12eV$: a slight increase of the magnetic moment from 4.04 up to $4.15\mu_B$ is visible, while the maximum $E_B - E_F$ difference is of order of $100meV$. Therefore in the following calculations we take the values $U_{Ho} = 8eV$ and $J_{Ho} = 0.9eV$ for the Coulomb and exchange parameters, which agrees with the values reported in literature for metallic rare-earth compounds [38]. Using these values we performed calculations for three supercells containing 16 atoms in the case of $Co_8HoMn_3Si_4$, 32 atoms for $Co_{16}Mn_7HoSi_8$ and respectively 64 atoms for the $Co_{32}Mn_{15}HoSi_{16}$ cell. In Fig. 6 we show the spin resolved density of states for the two largest supercells. In the inset the concentration dependence of the Ho spin moment is presented for all three supercells. Again one can see that the results does not significantly change with the dimension of the cells. Therefore for computational convenience, and in order to obtain the value for the orbital

magnetic moment of Ho, we carried out the LDA+U calculation including both spin-orbit coupling and non-collinearity effects for the smallest supercell in discussion $\text{Co}_8\text{HoMn}_3\text{Si}_4$. Our calculation yields a self-consistent collinear antiparallel configuration of the holmium moments with respect to the transition metal moments, with values of spin and orbital moments of $3.917\mu_B$ and $5.914\mu_B$, respectively. The total magnetic moment ($9.83\mu_B$) is close to the usual value determined by neutron diffraction in compounds having cubic structure with similar space group, such as HoFe_2 [41]. Similarly to the Ho spin moments, which were shown not to change significantly from one supercell to the other, we do not expect significant changes of the Ho orbital moments as well, since the magnitude of Ho spin-orbit coupling does not change appreciably with concentration, provided one uses the same type of structure and similar lattice parameters. For this reason, it is justified to neglect spin-orbit coupling for the band structure calculation in the larger supercell presented below. In this case, in order to compare the total magnetic moment with the experimentally measured values, the orbital magnetic moment calculated above for the smaller supercell is then added to the spin moments to obtain the results shown in Table II.

As discussed above, in the case of Co_2MnSi rare-earth impurities can in principle enter in both the Co and the Mn- sublattices. For this reason, we present results for the electronic-structure calculations carried out on the $\text{Co}_{16}\text{Mn}_7\text{HoSi}_8$ supercell to simulate Ho substitution at the Mn sites, and for a $\text{Co}_{15}\text{HoMn}_8\text{Si}_8$ cell when Ho replaces Co. The self-consistent calculations were performed assuming a collinear, parallel and respectively anti-parallel orientation of the $\text{Ho}(4f)$ magnetic moment with respect to the $\text{Mn/Co}(3d)$ ones. The resulting density of states for $\text{Co}_{16}\text{Mn}_7\text{HoSi}_8$ with both parallel and antiparallel orientation between $\text{Ho}(4f)$ - $\text{Mn}(3d)$ moments are plotted in Fig. 7. The half-metallic state is stable in both cases, with a gap of similar magnitude. However, the presence of rare-earth impurities induces a redistribution of states such that the Fermi level moves slightly towards the center of the gap, thus making the half-metallic state more stable. It is important to mention that in the case of $\text{Co}_{16}\text{Mn}_7\text{HoSi}_8$ $\text{Ho}(4f)$ -orbitals do not hybridize with the $3d$ orbitals near the Fermi level, the behaviour of DOS near E_F is very similar to the undoped case, so the nature of carriers around E_F is not changed.

To compute the values of the $\text{Ho}(4f)$ - $\text{Mn}(3d)$ exchange coupling, we use a two-sublattice model that describes the sublattice of $\text{Ho}(4f)$ spin moments as being antiparalely or parallely oriented to the $\text{Mn}(3d)$ spins sublattice. In this simplified model the exchange coupling, J ,

corresponds to the intersublattice couplings. In this model the Mn(3d) and the Ho(4f)-states are treated within a mean field LDA+U approach, whereas the Ho(4f)-Mn(3d) interaction was treated as a perturbation. The corresponding mean-field Hamiltonian can be written in the form:

$$H \approx H_{LDA+U} - J \sum_{i,\delta} \sigma_i^{3d} S_{i+\delta}^f \quad (1)$$

Here, σ_i^{3d} represents the spin operator of the 3d electrons at site \mathbf{r}_i , and $S_{i+\delta}^f$ the spin of the 4f shell at the site $\mathbf{r}_{i+\delta}$. Within this model the Mn(3d) local moment fluctuation could be quenched by a strong Ho(4f)-Mn(3d) coupling affecting the magnon excitations of the 3d conduction electron spins of the Mn-sublattice. Given the geometry of the cell, when Ho is substituted into the Mn- sublattice, twelve pairs of Ho(4f)-Mn(3d) are formed. The corresponding Ho(4f)-Mn(3d) coupling constant is calculated as the energy difference between the parallel E_P and the antiparallel E_{AP} configuration. In this way, we obtain a value of $J \simeq 88K$. In analysing the behaviour of exchange constants in Co_2MnSi , it was recently pointed out that Co-Mn interactions are responsible for the stability of the ferromagnetism [10, 11], in particular the main exchange parameter corresponds to the nearest-neighbour Co1-Mn interaction which already gives 70% of the of the total contribution to J being about ten times larger than the Co-Co and Mn-Mn interactions [40, 42]. For the small Ho content in the Co_2MnSi , it is shown experimentally , see table Tab.I, that the ferromagnetic Curie temperature is not significantly reduced, so one can conclude that the Co1-Mn interaction is not considerably affected, and in particular this interaction dominates over the 3d – 4f coupling.

The resulting total magnetic moments of the supercell, taking into account orbital Ho moments as well, were $26.09\mu_B$ and $45.91\mu_B$ for antiparallel and parallel orientations of Ho with respect to the Mn and Co moments, respectively.

As shown in Ref. [39] and briefly described above (Fig. 4), the minority gap is formed by the triply degenerate Co-Co anti-bonding t_{2g} and the double degenerate Co-Co anti-bonding e_g . Thus, it is expected that a substitution in the Co sublattice would have a stronger effect on the electronic structure than the substitution in the Mn sublattice, described above.

Results of the selfconsistent spin polarized LDA+U calculation for the $\text{Co}_{15}\text{HoMn}_8\text{Si}_8$ supercell, in which Ho atoms substitutes one of the cobalt sites is shown in Fig.8. Identical results are obtained when Ho substitutes Co1 or Co2 because cobalt occupies equivalent

sites. The magnetic moments per formula unit in the doped material show a departure from the integer values corresponding to the half-metallic case. For Ho impurity on the cobalt site, neglecting the orbital contribution, in the anti-parallel $4f - 3d$ configuration we obtain $\mu_{Ho/Co1}^{(AP)} = 34.81\mu_B$ per supercell, while for the parallel case we have $\mu_{Ho/Co1}^{(P)} = 41.87\mu_B$ per supercell. Also in this case, the antiparallel configuration is the most stable one, in agreement with the magnetic measurements discussed above. An interesting aspect is that, in contrast to the case of substitution at the Mn site, substitution at Co sites fills the minority-spin gap, as can be seen in Fig. 8. Notice that Ho($4f$) and ($5d$) states shown in Fig. 8 were multiplied by ten in order to evidence possible hybridization effects. As one can see (Fig. 8) the Ho($4f$) states show no significant contribution in a large energy range ($E_F \pm 3eV$) around the Fermi level. Occupied and empty Ho($4f$) states are present in the energy range -8 to -6eV, and 2 to 4eV respectively, not shown in Fig. 8. The anti-bonding $Co^{3d}(e_g)$ -Ho $^{5d}(e_g)$ states appear for both parallel and anti-parallel configurations above the Fermi level up to energies $E_F + 0.2eV$ and these states determine the shift of the Fermi level within the conduction band, thus the closure of the half-metallic gap.

Notice that as result of hybridization effects, a small negative magnetic moment is induced on silicon. Values of $-0.017\mu_B$ are obtained when Ho is located on Mn sites and $-0.047\mu_B$ when Ho replaces Co. The computed magnetic moments of the atoms when Ho replaces Mn or Co in both the antiparallel and parallel alignments are listed in Table II. The computed magnetic moments per formula unit for $Co_2Mn_{7/8}Ho_{1/8}Si$ and $Co_{15/8}MnHo_{1/8}Si$ are also shown. These compare reasonably with experimental data, when corrections for different compositions are made. This is done by extrapolating the experimental data obtained with $x = 0.05$ and 0.10 to the theoretically computed case $x = 0.125$. A rather good agreement between computed and experimental values is obtained when the holmium replaces cobalt atoms in the antiparallel configuration, while a worse agreement is shown when holmium replaces manganese, see Tab.II, although energetically substitution in the former way is less favorable.

III. CONCLUSION

The behavior of spin polarization as a function of temperature is an important issue for many spintronic materials. In our recent paper [24], we interpreted the measured drastic

depolarization in Co_2MnSi as due to the existence of non-quasiparticle states just above the Fermi level. Since the origin of these states is related to the electron-magnon interaction, a possibility to reduce this depolarisation effect would be to quench the magnon excitations, while keeping the minority spin channel gapped. This possibility was already discussed in connection to light-rare earth (Nd) insertion into the host Co_2MnSi [35], supporting the validity of the proposed scenario. In the present work, we first demonstrate experimentally the possibility that a heavy rare-earth element (Ho) enters into the transition-metal sublattices in Co_2MnSi . In addition, we carried out an electronic-structure calculation whose results suggest that the half-metallicity is maintained when Ho replace Mn atom in an anti-parallel magnetic $\text{Ho}(4f)\text{-Mn}(3d)$ configuration. Since the calculated exchange coupling J turns out to be about $88K$, we expect that for temperatures smaller than J such a substitution could in principle influence the magnonic excitations, while at the same time leaving the half-metallic gap unchanged. On the other hand, our results show that when the substitution takes place at Co sites, the minority-spin gap is filled, and half-metallicity is lost.

The present calculations does not take into account relaxation effects which might appear as a result of substitution. This will constitute the subject of future investigations. Dynamic correlation effects are also expected to be important. In particular, it would be interesting to investigate up to which extent magnonic excitations and electron-magnon interactions are affected by Ho substitution. We plan to investigate this effect in the future.

M.I. Katsnelson and A.I. Lichtenstein are acknowledged for useful discussions. LC and EA acknowledge financial support by the Austrian science fund (FWF project P18505-N16).

-
- [1] R. A. de Groot, F. M. Mueller, P. G. van Engen, and K. H. J. Buschow, *Phys. Rev. Lett.* **50**, 2024 (1983).
 - [2] M. I. Katsnelson *et al.*, *Reviews of Modern Physics* **80**, 315 (2008).
 - [3] R. A. de Groot, A. M. van der Kraan, and K. H. J. Buschow, *J. Magn. Magn. Mater.* **61**, 330 (1986).
 - [4] R. A. de Groot, *Physica B* **172**, 45 (1991).
 - [5] P. A. Dowben and R. Skomski, *Journal of Applied Physics* **93**, 7948 (2003).
 - [6] A. R. Machintosh and O. K. Andersen, in *Electrons at the Fermi surface*, edited by M. Spring-

- ford (Cambridge Univ. Press., London, 1980).
- [7] A. I. Liechtenstein, M. I. Katsnelson, V. P. Antropov, and V. A. Gubanov, J. Mag. Mag. Matt. **67**, 65 (1987).
 - [8] D. Orgassa, H. Fujiwara, T. C. Schulthess, and W. H. Butler, Phys. Rev. B **60**, 13237 (1999).
 - [9] D. Orgassa, H. Fujiwara, T. C. Schulthess, and W. H. Butler, J. Appl. Phys. **87**, 5870 (2000).
 - [10] E. Sasioglu, L. M. Sandratskii, and P. Bruno, J. Phys.: Condens. Matter **17**, 995 (2005).
 - [11] E. Sasioglu, L. M. Sandratskii, P. Bruno, and I. Galanakis, Phys. Rev. B **72**, 184415 (2005).
 - [12] R. Skomski and P. A. Dowben, Europhys. Lett., **58**, 544 (2002).
 - [13] V. Y. Irkhin and M. I. Katsnelson, Sov. Phys. - Solid State **25**, 1947 (1983).
 - [14] D. M. Edwards and J. A. Hertz, Journal of Physics F-Metal Physics **3**, 2191 (1973).
 - [15] V. Y. Irkhin and M. I. Katsnelson, J. Phys.: Condens. Matter **2**, 7151 (1990).
 - [16] V. Y. Irkhin and M. I. Katsnelson, Phys. Usp. **37**, 659 (1994).
 - [17] V. Y. Irkhin and M. I. Katsnelson, Phys. Rev. B **73**, 104429 (2006).
 - [18] V. Y. Irkhin and M. I. Katsnelson, Eur. Phys. J. B **43**, 479 (2005).
 - [19] G. Tkachov, E. McCann, and V. I. Fal'ko, Phys. Rev. B **65**, 024519 (2001).
 - [20] G. Kotliar *et al.*, Rev. Mod. Phys. **78**, 865 (2006).
 - [21] L. Chioncel, M. I. Katsnelson, R. A. de Groot, and A. I. Lichtenstein, Phys. Rev. B **68**, 144425 (2003).
 - [22] L. Chioncel, E. Arrigoni, M. I. Katsnelson, and A. I. Lichtenstein, Phys. Rev. Lett. **96**, 137203 (2006).
 - [23] L. Chioncel, E. Arrigoni, M. I. Katsnelson, and A. I. Lichtenstein, Phys. Rev. B **79**, 125123 (2009).
 - [24] L. Chioncel *et al.*, Phys. Rev. Lett. **100**, 086402 (2008).
 - [25] L. Chioncel *et al.*, Phys. Rev. B **71**, 085111 (2005).
 - [26] L. Chioncel *et al.*, Phys. Rev. Lett. **96**, 197203 (2006).
 - [27] L. Chioncel *et al.*, Phys. Rev. B **75**, 140406 (2007).
 - [28] G. H. Fecher *et al.*, Appl. Phys. Lett. **99**, 08J106 (2006).
 - [29] S. Wurmehl *et al.*, Journal of Applied Physics **99**, 08J103 (2006).
 - [30] H. C. Kandpal, G. H. Fecher, C. Felser, and G. Schönhense, Phys. Rev. B **73**, 094422 (2006).
 - [31] M. P. Raphael *et al.*, Appl. Phys. Lett. **79**, 4396 (2001).
 - [32] J. J. Attema *et al.*, J. Phys.: Condens. Matter **16**, S5517 (2004).

- [33] L. Chioncel, Finite Temperature Electronic Structure, beyond Local Density Approximation, PhD thesis, University Nijmegen, 2004.
- [34] R. Tetean *et al.*, Appl. Surf. Science **255**, 685 (2008).
- [35] A. Rajanikanth, Y. K. Takahashi, and K. Hono, Journal of Applied Physics **105**, 063916 (2009).
- [36] P. J. Brown, K. U. Neumann, P. J. Webster, and K. R. A. Ziebeck, J. Phys.: Condens. Matter **12**, 1827 (2000).
- [37] O. K. Andersen and O. Jepsen, Phys. Rev. Lett. **53**, 2571 (1984).
- [38] V. I. Anisimov, F. Aryasetiawan, and A. I. Lichtenstein, Journal of Physics: Condensed Matter **9**, 767 (1997).
- [39] I. Galanakis, P. Mavropoulos, and P. H. Dederichs, J. Phys. D: Appl. Phys. **39**, 765 (2006).
- [40] J. Kübler, G. H. Fecher, and C. Felser, Phys. Rev. B **76**, 024414 (2007).
- [41] E. Burzo, A. Chelkowski, and H. R. Kirchmayr, in *Landolt Börnstein Handbook* (Springer Verlag, Heidelberg, 1990), Vol. 19d2, p. 130.
- [42] Y. Kurtulus, R. Dronskowski, G. D. Samolyuk, and V. P. Antropov, Phys. Rev. B **71**, 014425 (2005).

Alloy	Lattice constant (\AA)	Saturation magnetization at 4.2K (μ_B/fu)	T_c (K)
$Co_2Mn_{0.95}Ho_{0.05}Si$	5.651(2)	4.40 ± 0.07	984
$Co_2Mn_{0.90}Ho_{0.10}Si$	5.658(2)	4.05 ± 0.07	982
$Co_{1.95}Ho_{0.05}MnSi$	5.655(3)	4.30 ± 0.07	983
$Co_{1.90}Ho_{0.10}MnSi$	5.659(2)	3.94 ± 0.07	982

TABLE I: Lattice parameters, saturation magnetizations and Curie temperatures for the studied compounds.

Sample	Magnetic coupling	Computed magnetic moments (μ_B)					Experimental*
		M_{Co}	M_{Mn}	M_{Ho}	M_{Si}	M_{tot}	
Co_2MnSi		1.003	3.026	-	-0.03	5.002	-
$Co_2Ho_{1/8}Mn_{7/8}Si$	P	1.013	2.866	9.779	-0.018	5.738	-
$Co_2Ho_{1/8}Mn_{7/8}Si$	AP	1.009	2.866	-9.979	-0.017	3.261	3.87 ± 0.2
$Co_{15/8}Ho_{1/8}MnSi$	AP(Co1/Co2)	0.941	3.110	-9.625	-0.047	3.626	3.76 ± 0.1

TABLE II: Calculated magnetic moments for different Ho-substituted compounds. The experimental data * are obtained by extrapolating the measured values ($x = 0.05$ and 0.10) to $x = 0.125$ composition.

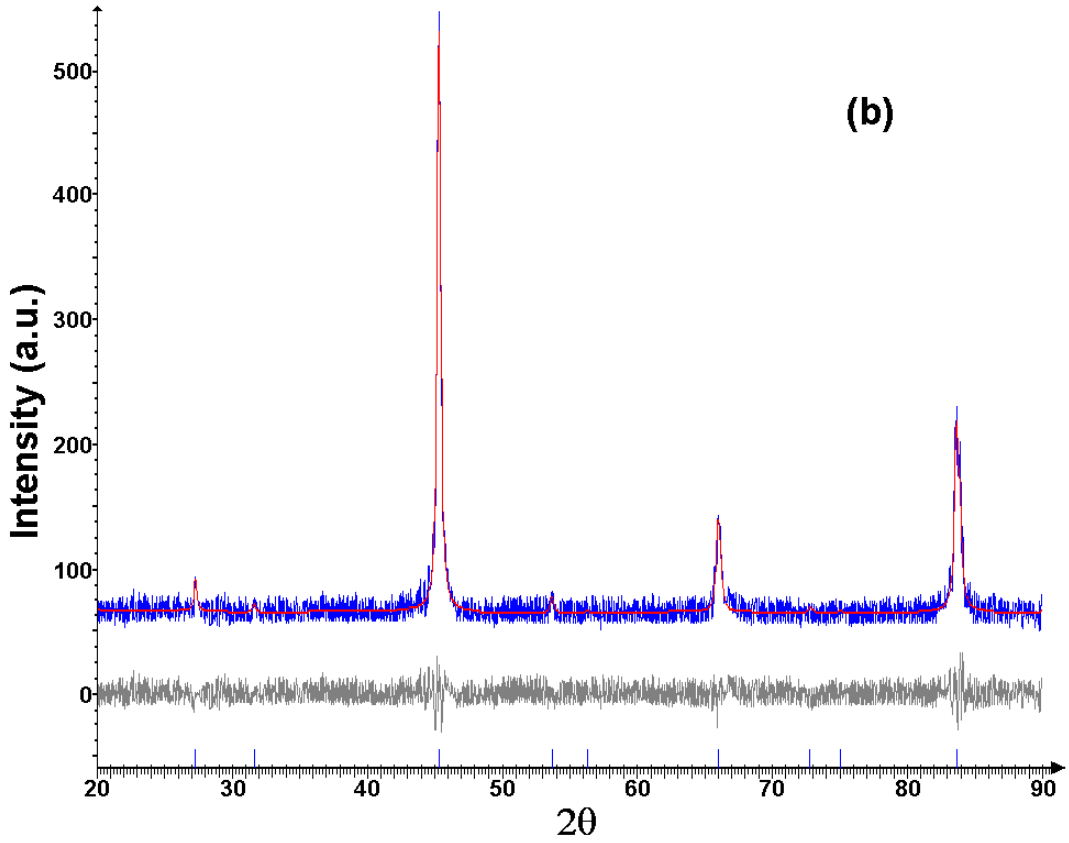
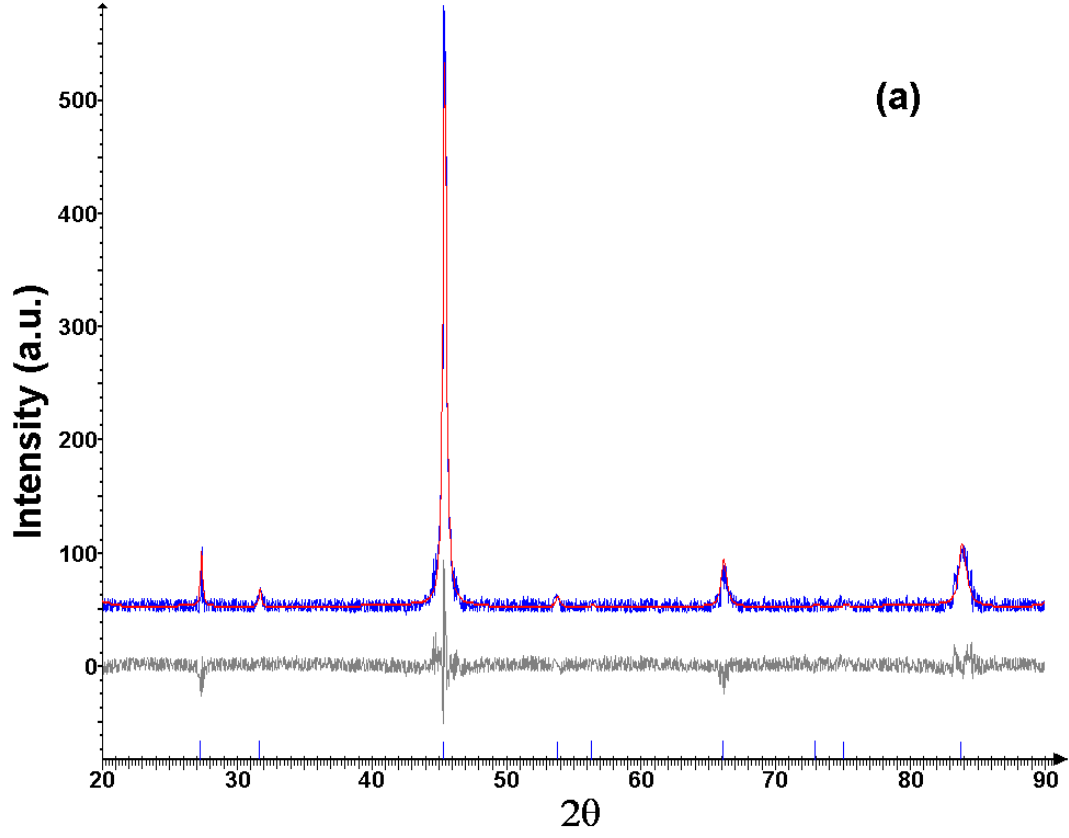


FIG. 1: (Color online) Refined X-ray spectra for $\text{Co}_2\text{Mn}_{1-x}\text{Ho}_x\text{Si}$ samples with $x=0.05$ (a) and 0.1 (b).

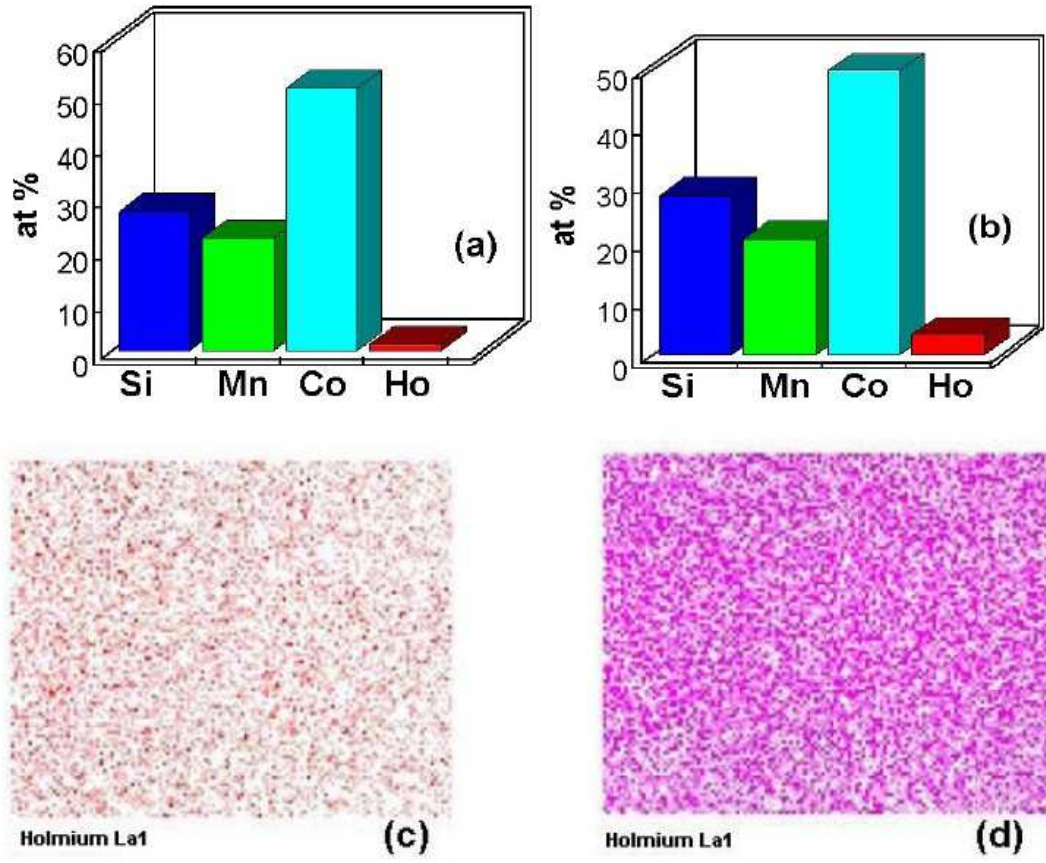


FIG. 2: (Color online) Compositions of the $\text{Co}_2\text{Mn}_{0.95}\text{Ho}_{0.05}\text{Si}$ (a) and $\text{Co}_2\text{Mn}_{0.9}\text{Ho}_{0.1}\text{Si}$ (b) samples as well as the holmium distributions in $\text{Co}_2\text{Mn}_{0.95}\text{Ho}_{0.05}\text{Si}$ (c) and $\text{Co}_2\text{Mn}_{0.9}\text{Ho}_{0.1}\text{Si}$ (d) samples.

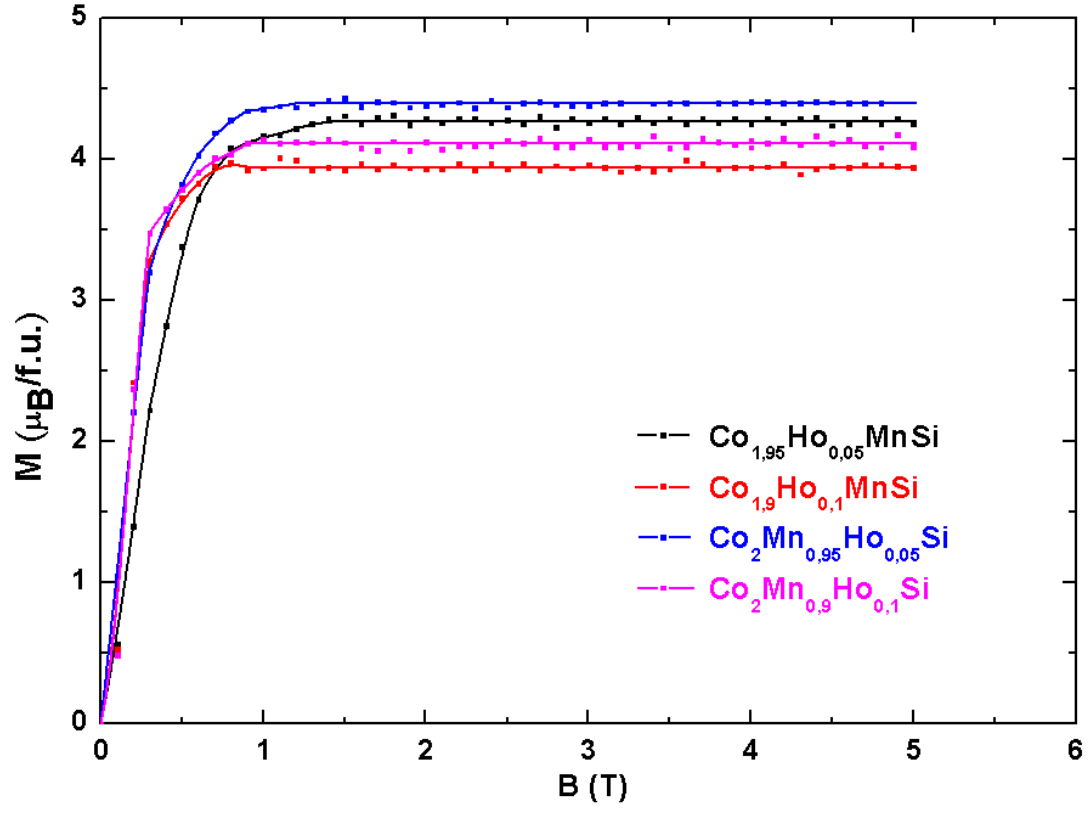


FIG. 3: (Color online) Magnetization isotherms at 4.2 K.

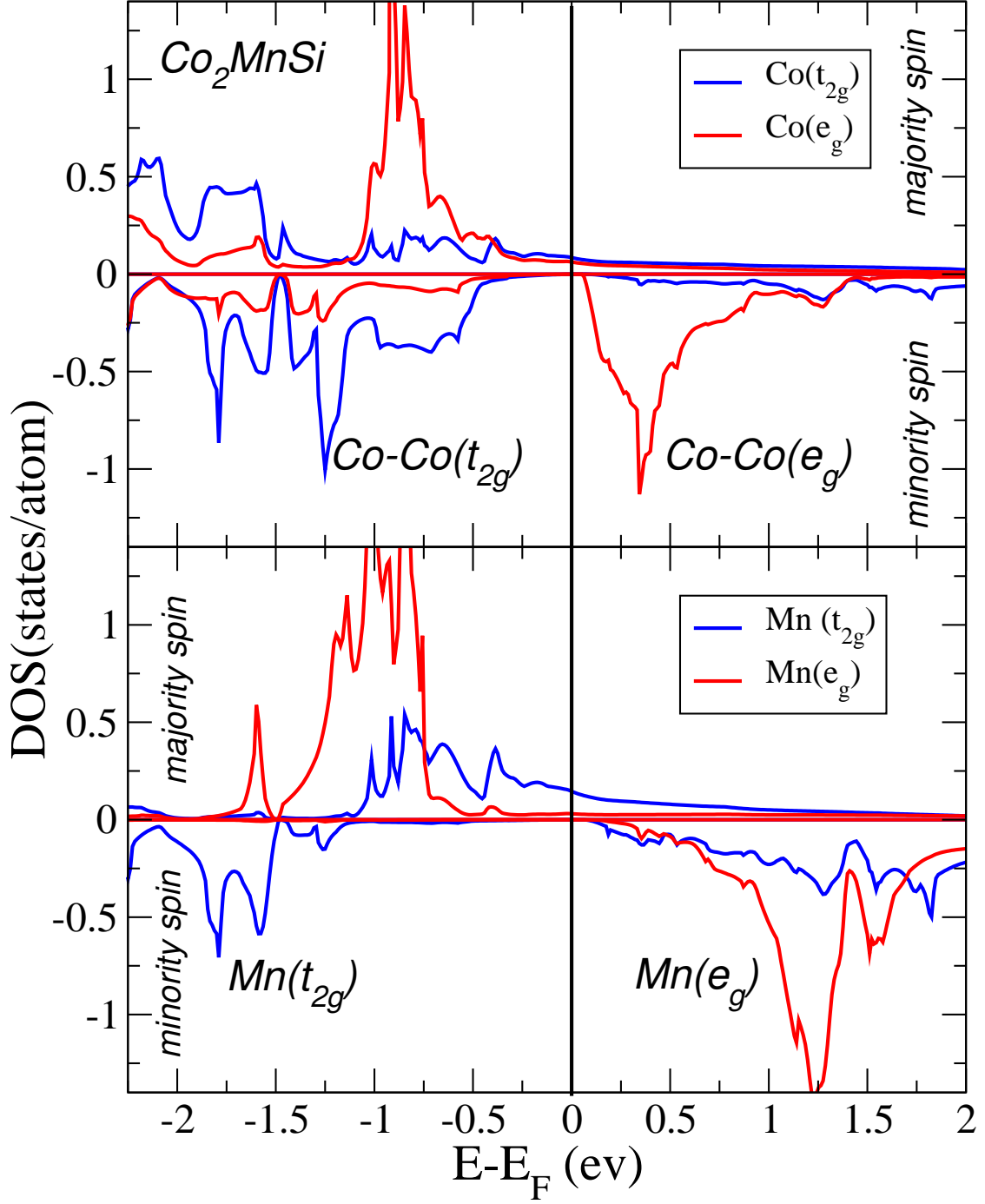


FIG. 4: (Color online) Spin and orbital resolved density of states of the (stoichiometric) Co_2MnSi full-Heusler alloy obtained by spin-polarized LDA. The half-metallic gap in the minority spin channel is formed between the hybrid $\text{Co-Co}(t_{2g})$ and $\text{Co-Co}(e_g)$ orbitals. No significant Mn-orbitals contributions to the edges of the minority spin gap can be seen in the lower panel.

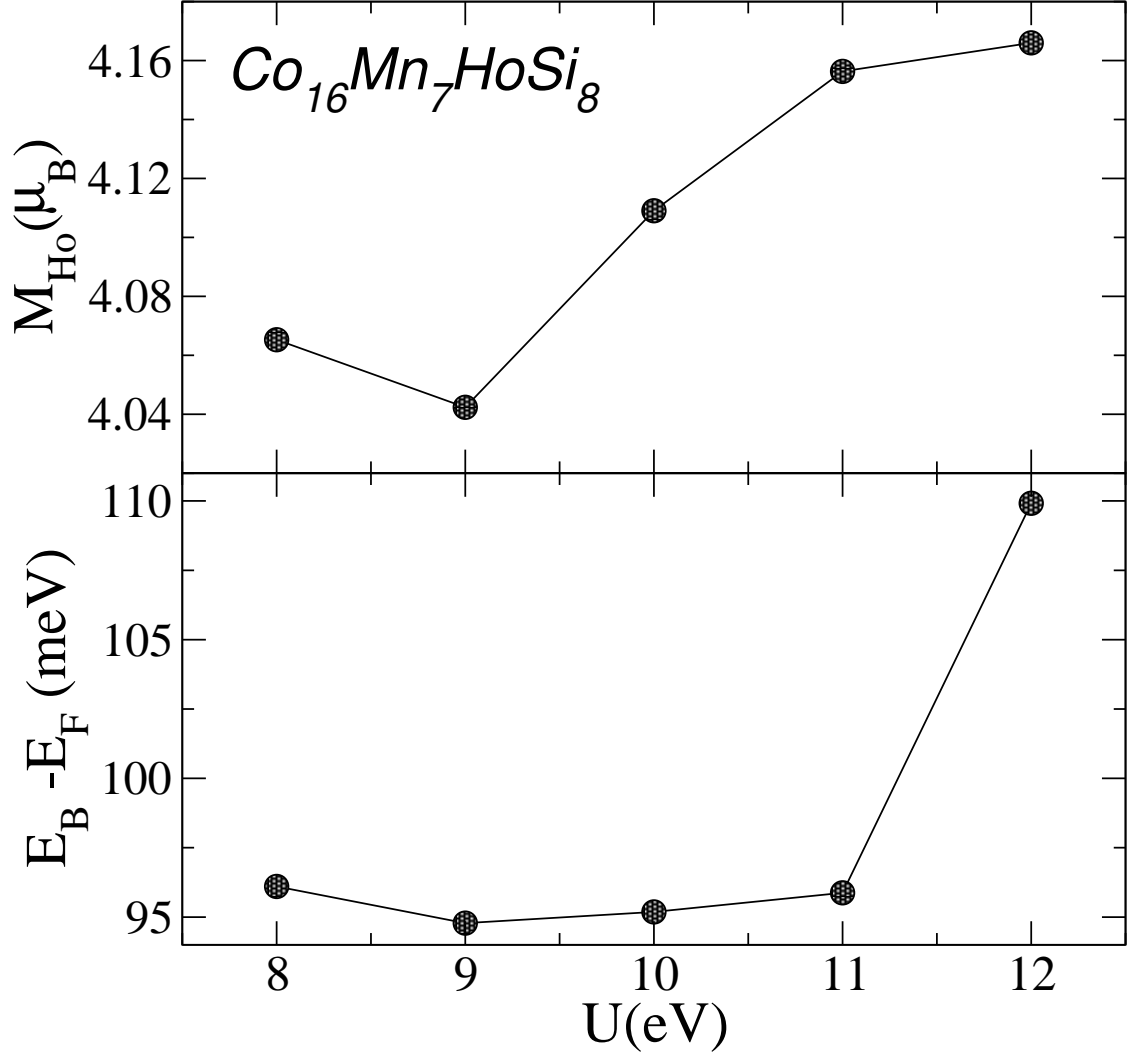


FIG. 5: (Color online) The minority spin half-metallic gap as function of the average Coulomb parameter U . No significant U dependence is present which demonstrates the lack on 4f-3d hybridizations around the Fermi level.

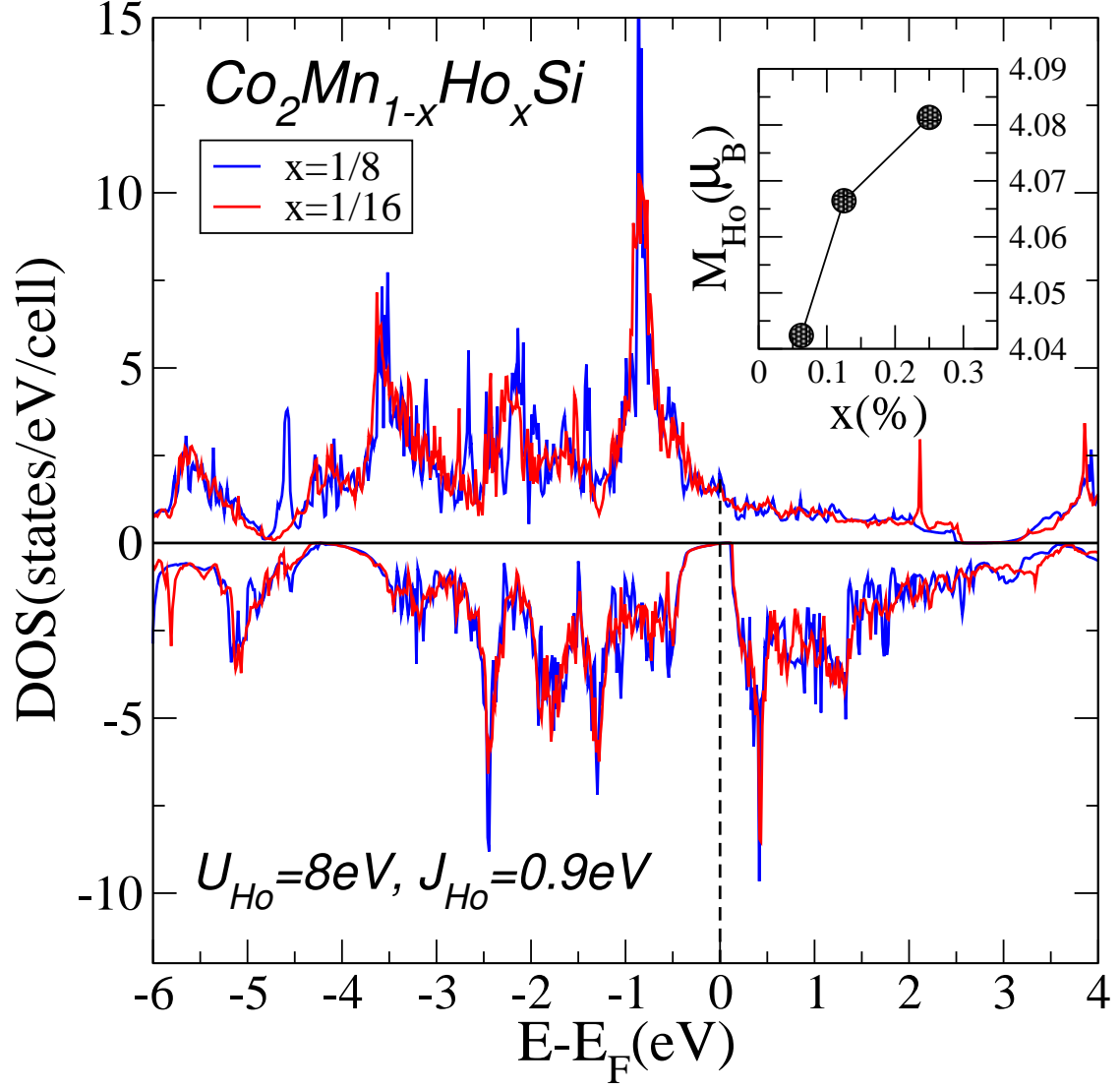


FIG. 6: (Color online) Spin resolved density of states for different eight respectively 16 times larger supercells of Co_2MnSi . The inset shows the composition dependence Ho magnetic spin moments. No essential changes are visible around the Fermi level.

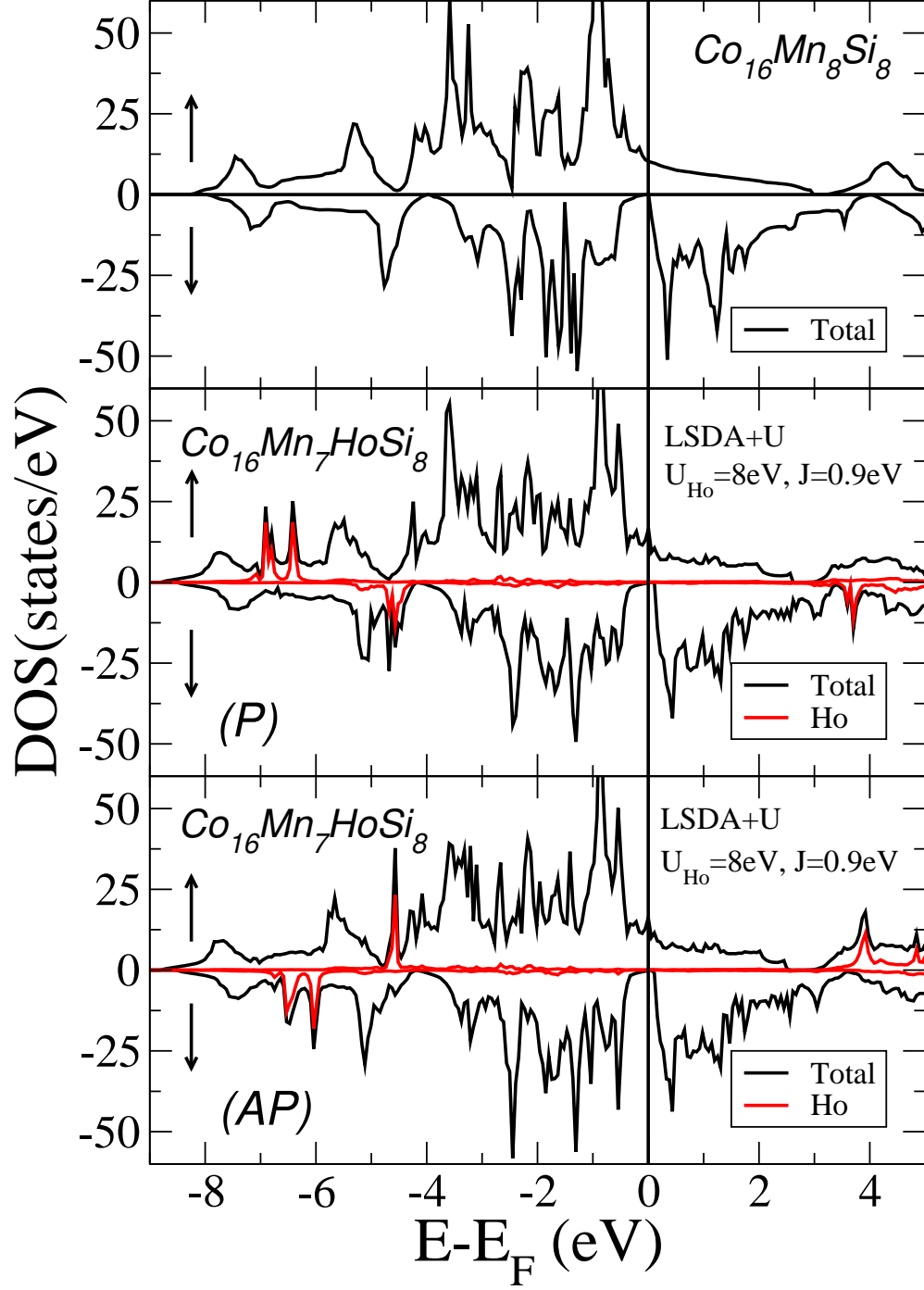


FIG. 7: (Color online) Spin resolved density of states of the $\text{Co}_{16}\text{Mn}_7\text{HoSi}_8$ supercell in the parallel (P) and anti-parallel (AP) configuration between $\text{Ho}(4f) - \text{Mn}(3d)$ moments. For comparison, the Co_2MnSi density of states is also plotted. In the presence of Ho, Fermi level shifts towards the middle of the minority-spin gap, however the magnitude of the gap remains unchanged.

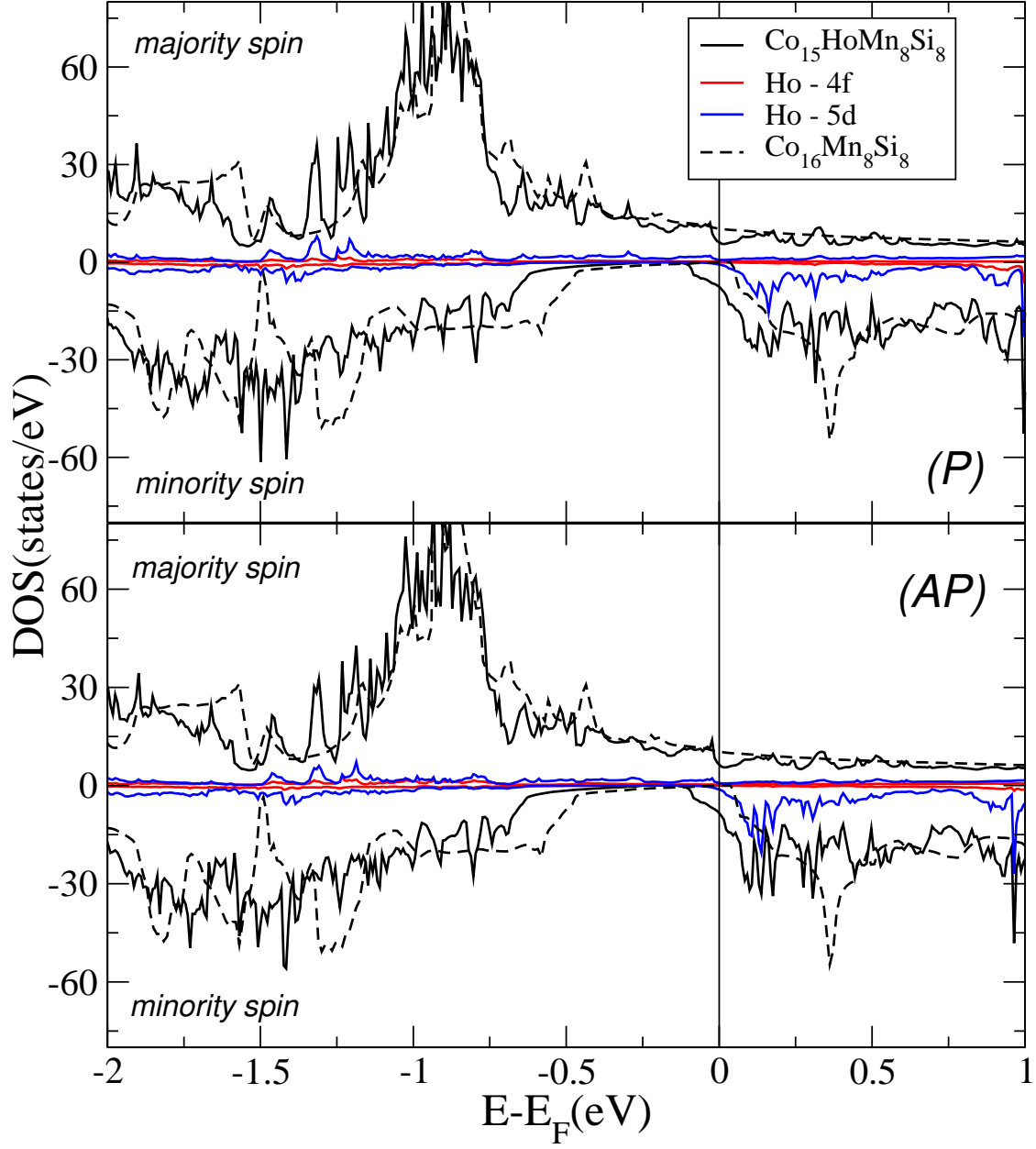


FIG. 8: (Color online) Spin resolved density of states around the Fermi level for the $\text{Co}_{15}\text{HoMn}_8\text{Si}_8$ supercell, in the parallel and anti-parallel configurations, where Ho is substituted into Co1 lattice sites. The Ho-4f and -5d states are magnified by a factor of ten in order to evidence hybridization effects. The minority-spin gap is closed due to the $\text{Co}^{3d}(e_g)\text{-Ho}^{5d}(e_g)$ anti-bonding coupling which pushes the Fermi level within the conduction band.